



HAL
open science

Cooperative Redox Transitions Drive Electrocatalysis of the Oxygen Evolution Reaction on Cobalt–Iron Core–Shell Nanoparticles

Lisa Royer, Antoine Bonnefont, Tristan Asset, Benjamin Rotonelli, Juan-Jesús Velasco-Vélez, Steven Holdcroft, Simon Hettler, Raul Arenal, Benoit Pichon, Elena Savinova

► To cite this version:

Lisa Royer, Antoine Bonnefont, Tristan Asset, Benjamin Rotonelli, Juan-Jesús Velasco-Vélez, et al.. Cooperative Redox Transitions Drive Electrocatalysis of the Oxygen Evolution Reaction on Cobalt–Iron Core–Shell Nanoparticles. *ACS Catalysis*, 2022, 13 (1), pp.280-286. 10.1021/acscatal.2c04512 . hal-04296198

HAL Id: hal-04296198

<https://hal.science/hal-04296198>

Submitted on 21 Nov 2023

HAL is a multi-disciplinary open access archive for the deposit and dissemination of scientific research documents, whether they are published or not. The documents may come from teaching and research institutions in France or abroad, or from public or private research centers.

L'archive ouverte pluridisciplinaire **HAL**, est destinée au dépôt et à la diffusion de documents scientifiques de niveau recherche, publiés ou non, émanant des établissements d'enseignement et de recherche français ou étrangers, des laboratoires publics ou privés.

Cooperative redox transitions drive electrocatalysis of the oxygen evolution reaction on cobalt-iron core- shell nanoparticles

*Lisa Royer^{1,10}, Antoine Bonnefont*², Tristan Asset¹, Benjamin Rotonelli¹, Juan Velasco Velez^{3,4,5}, Steven Holdcroft⁶, Simon Hettler^{7,8}, Raul Arenal^{7,8,9}, Benoit Pichon^{10,11}, Elena Savinova¹*

¹ ICPEES, UMR 7515 CNRS-ECPM-Université de Strasbourg, 25, rue Becquerel, F 67087
Strasbourg Cedex 2, France

² Institut de Chimie, UMR 7177, CNRS-Université de Strasbourg, 4 rue Blaise Pascal, CS 90032,
67081 Strasbourg cedex, France

³ Fritz-Haber-Institute of the Max-Planck-Society, Faradayweg 4-6, 14195 Berlin, Germany

⁴ Department of Heterogeneous Reactions, Max Planck Institute for Chemical Energy Conversion,
45470 Mülheim an der Ruhr, Germany.

⁵ ALBA Synchrotron Light Source, Cerdanyola del Vallés (Barcelona) 08290, Spain.

⁶ Department of Chemistry, Simon Fraser University, 8888 University Drive, Burnaby, BC, V5A
1S6, Canada

⁷ Instituto de Nanociencia y Materiales de Aragon (INMA), CSIC-Universidad de Zaragoza,
Calle Pedro Cerbuna 12, 50009 Zaragoza, Spain

⁸ Laboratorio de Microscopías Avanzadas (LMA), Universidad de Zaragoza, Calle Mariano
Esquillor, 50018 Zaragoza, Spain

⁹ARAID Foundation, 50018 Zaragoza, Spain

¹⁰ IPCMS Université de Strasbourg, CNRS, Institut de Physique et Chimie des Matériaux de
Strasbourg, UMR 7504, Strasbourg, F-67034 France

¹¹ Institut Universitaire de France, 75231 Paris Cedex 05, France

AUTHOR INFORMATION

Corresponding Author

Antoine Bonnefont : pierre-antoine.bonnefont@grenoble-inp.fr

Institut de Chimie, UMR 7177, CNRS-Université de Strasbourg, 4 rue Blaise Pascal, CS 90032,
67081 Strasbourg cedex, France

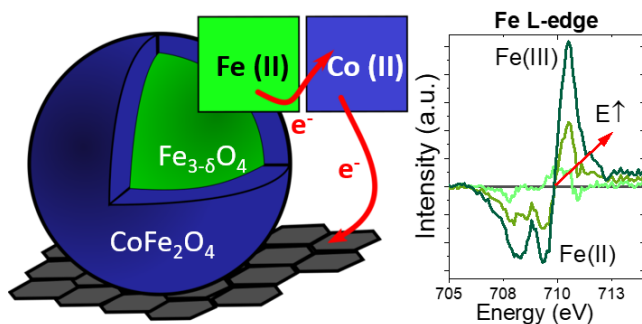
Present address: University Grenoble Alpes, University Savoie Mont Blanc CNRS, Grenoble INP
(Institute of Engineering, University Grenoble Alpes), LEPMI, 38000 Grenoble, France

ABSTRACT

Transition metal oxides are promising materials for the development of cost-effective catalysts for the oxygen evolution reaction (OER) in alkaline media. Understanding the catalysts'

transformations occurring during the harsh oxidative conditions of the OER remains a bottleneck for the development of stable and active catalysts. Here, we studied redox transformations of core-shell $\text{Fe}_3\text{O}_4@\text{CoFe}_2\text{O}_4$ oxide nanoparticles over a wide range of potentials by using *operando* near-edge X-ray absorption fine structure (NEXAFS) spectroscopy in total electron yield (TEY) detection mode. The analysis of the NEXAFS spectra reveals that the Fe_3O_4 core strongly affects the surface chemistry of the CoFe_2O_4 shell under the OER conditions. The spinel structure of the particles with Co (II) in the shell is preserved at potentials as high as 1.8 V vs. RHE, at which Co (II) is expected to be oxidized into Co (III); whereas Fe (II) in the core is reversibly oxidized to Fe (III).

TOC GRAPHICS



KEYWORDS: electrochemistry, electrocatalysis, *operando* NEXAFS, Oxygen Evolution Reaction (OER), core-shell nanoparticles, cobalt ferrite

Anion exchange membrane water electrolysis (AEMWE) is an attractive alternative to the proton exchange membrane counterpart as it allows the replacement of iridium or ruthenium at the

anode with more abundant 3d (Ni, Co, Fe, Mn) transition metal oxides (TMO)^{1,2}. TMOs with spinel structure constitute a promising class of oxygen evolution reaction (OER) catalysts due to their relatively low synthesis temperature (allowing preparation of high surface area catalysts without coalescence), and their composition-dependent and widely tunable properties thus allowing to attain high OER activity. However, the evolution of the surface structure and the composition under the OER conditions and hence the nature of the active sites are not fully understood yet. These knowledge gaps hamper building correlations between the chemical structure of materials on the one hand and their OER activity/durability on the other hand, ultimately impeding the development of active and stable catalysts for the anode of the AEMWE.

Bergmann *et al.*³ studied nanocrystalline Co₃O₄ films during the OER using *in situ* X-ray diffraction and ‘quasi-in situ’ absorption spectroscopy (samples were freeze-quenched under potential control). They found that in the potential interval of the OER, Co (II) ions were oxidized to octahedrally (Oh) coordinated, di- μ -O(H)-bridged Co (III/IV) species resulting in a reversible formation of a sub-nanometer thick amorphous CoO_x(OH)_y shell. In contrast, Ortiz-Pena *et al.*⁴ studied Co₃O₄ nanoparticles (NPs) *in situ* by transmission electron microscopy (TEM) under potential control (EC-TEM) and found that this amorphization is irreversible. Also, Reikowski *et al.*⁵ applied *operando* surface X-ray diffraction to study structurally well-defined epitaxial cobalt oxide Co₃O₄(111) thin films electrodeposited on Au (111). They observed fast and fully reversible Co₃O₄ (111)/CoOOH (001) transformation at potentials 300 mV negative of the ‘onset’ of the OER, and thus concluded that the observed structural transformation was potential rather than OER-driven. By comparing the OER activity of Co₃O₄ (111) and CoOOH (001) epitaxial crystalline films, the authors argued against di- μ -oxo bridged Co cations being responsible for the OER activity of Co oxides. For Co(OH)₂ particles, Mefford *et al.*⁶, by using *operando* scanning

probe and X-ray microscopy techniques, documented Co(II) into Co(III) oxidation leading to the formation of β -CoOOH under OER conditions and concluded that Co(III) at the particle surface were the OER active catalytic sites. Recently, Haase *et al.*⁷ studied transformations of $\text{CoO}_x(\text{OH})_y$ NPs with the average size ranging from 1.6 to 9.3 nm during the OER with *operando* hard X-ray absorption spectroscopy and density functional theory (DFT). While confirming an increase of the average cobalt oxidation state from II to III+ δ , the authors arrived at the conclusion that during the OER, an electron ‘hole’ resides on oxygen (the so-called ‘anion-redox’ OER mechanism) ions rather than Co cations (hence Co (IV) species do not form), leading to the formation of electron-deficient ‘oxyl’ species (similar to what has been previously proposed for IrO_x -catalyzed OER^{8,9}). From the aforementioned works, it appears that (i) the oxidation degree of the Co during the OER, namely the occurrence of the Co (II) to Co (III) and Co (III) to Co (IV) transitions, and (ii) the formation of the CoOOH phase and its reversibility, are rather controversial in the literature. This complexifies even further when addressing the Co-Fe based catalysts for the OER.

Indeed, several studies have revealed the crucial role of iron in enhancing the OER activity of Co- and Ni-based TMO¹⁰ catalysts with further controversies regarding the reasons for this enhancement. Since iron oxide has a low activity towards the OER, it was suggested that a synergetic effect between iron and other TMs such as nickel or cobalt¹¹ lies at the origin of the observed enhancement. Using Hubbard model DFT+U calculations, Wang *et al.*¹² demonstrated that, for Fe-doped Ni hydroxide, a local arrangement of Fe (III) with two Ni (IV) ions plays an important role in the OER activity, and that charge transfer during the OER occurs from Fe (III) to the OER intermediates. Xiao *et al.*¹³ also suggested a synergy between Fe and Ni where Fe (IV) catalyzes formation of an O radical intermediate and Ni (IV) catalyzes the O-O coupling. It was also argued that the presence of iron modifies the e_g orbital filling¹⁴, generating more active

materials towards the OER. DFT+U calculations were also applied to elucidate the influence of iron on the OER activity of Co_3O_4 ^{15,16}. They revealed influence of Fe on the oxidation state of Co and will be discussed in what follows. Although many studies have investigated transformations of cobalt-based catalysts during the OER, few have studied Co/Fe catalysts. Calvillo *et al.*¹⁷ studied the Fe K-edge and the Co K-edge to scrutinize the chemical and structure changes of a Co-Fe spinel powder during the OER and demonstrated that the samples suffered irreversible oxidation under the OER conditions leading to the formation of a layer consisting of Co_3O_4 , CoOOH , and Fe_2O_3 . They also stated that these were Co (II) cations in tetrahedral (Td) sites that were experiencing changes during the OER. Saddeler *et al.*¹⁸ recently studied cobalt iron spinel catalysts of different compositions and due to observed changes of the Co and Fe K-edge concluded that during the OER cobalt is oxidized to Co (III) while iron maintains its Fe (III) oxidation state.

In this work, we report on the cooperative redox behavior of core-shell, cobalt iron oxide nanoparticles ($\text{Fe}_3\text{O}_4@\text{CoFe}_2\text{O}_4$), possessing a conductive Fe_3O_4 core and an OER active CoFe_2O_4 shell. The use of core-shell nanoparticles where Co is present only in the shell has the advantage to drastically reduce the Co loading in the electrocatalyst. Furthermore, an improved OER performance may be expected if the particle core has beneficial impact on the shell properties^{19,20}. The core-shell structure with the catalytically active component localized in the shell is also very advantageous for operando investigations, since it significantly increases the surface sensitivity. Well-defined NPs with a narrow size distribution and controlled shape and composition both for the core and the core-shell were synthesized. The synthesis consisted in a seed-mediated growth based on the thermal decomposition of metal complexes as recently reported²¹. The obtained spinel $\text{Fe}_3\text{O}_4@\text{CoFe}_2\text{O}_4$ NPs (Figure 1 A) are homogeneous in size, shape, and composition and possess an average diameter of ~14 nm with a shell thickness of ~1.5 nm. Their diffractogram presents

peaks characteristic of an inverse spinel structure (Figure S1) in which Fe (II) occupies half of the Oh sites while Fe (III) occupies the other Oh sites and the Td sites in the Fe₃O₄ core. In the CoFe₂O₄ shell with inverse spinel structure, Co (II) occupies roughly half of the Oh sites while Fe (III) is in the rest of the Oh sites and the Td sites. Hence, Co is only present in the shell while Fe (II) is only present in the Fe₃O₄ core. For the *operando* NEXAFS study, 10 μL (4.2 μg) of NPs dispersed in chloroform were drop-cast either on the surface of a Fumatech anion exchange membrane (Fumasep® FAS-50) or on the surface of an Aemion® anion exchange membrane (Ionomr Innovations Inc.) and then covered by a graphene bilayer²², the latter establishing electric contact between the particles and the current collector. The shape of current-potential curves obtained with the two types of anion exchange membranes was similar (Figures 2A and S7). The membrane electrode assembly was used in the *operando* liquid spectro-electrochemical cell of the Innovative Station for In Situ Spectroscopy (ISIS) Beamline at Bessy synchrotron (Figure S5). A detailed description of the spectroelectrochemical cell can be found in ref²³. Complementary electrochemical measurements were performed in a conventional three-electrode electrochemical cell in 0.1 M NaOH electrolyte by depositing NPs on a glassy carbon (GC) disc (Figure S6). The core-shell nanoparticles exhibited OER activity of ~ 350 A/g_{oxide} at 1.65V vs. RHE (Figure S6) and this activity was multiplied by a factor of 10 if the current was normalized to the active component (cobalt mass). Their redox behavior was studied by *operando* NEXAFS in a wide potential interval (*cf.* cyclic voltammogram, CV, of Fe₃O₄@CoFe₂O₄ NPs acquired in the *operando* cell and presented in Figure 1 B) by monitoring the evolution of the near edge X-ray absorption fine structure (NEXAFS) spectra recorded for cobalt and iron L_{2,3}-edges and oxygen K-edge as a function of the applied potential. The Fe, Co L-edge, and O K-edge NEXAFS spectra were collected in total electron yield mode (TEY). The sampling depth of TEY measurements is

typically a few nanometers making this technique sensitive to the catalyst surface modifications during the OER.

We start our discussion with the analyses of redox transformations occurring at low electrode potentials. When the potential is decreased, a pair of anodic (P_A) and cathodic (P_C) redox peaks is observed in the CV at ca. 0.2 and at -0.2 V *vs.* the reversible hydrogen electrode (RHE), respectively (Figure 1C). The corresponding NEXAFS Fe $L_{2,3}$ -edges spectra measured in the interval from 1.0 down to -0.5 V *vs.* RHE are presented in Figure 1 C. For comparison, the cyclic voltammetry curve obtained for the core material (Fe_3O_4) is presented in Figure S8. The Fe L_3 and L_2 -edge peaks are observed in the intervals 709-712 eV and 720-725 eV respectively (Figure 1 C), and are sensitive to the valence and redox state of the atoms. At 1.0 V *vs.* RHE, the fine structure of the Fe L_3 -edge shows a second contribution at 709 eV, which is attributed to Fe (II), while the main peak at 711 eV is attributed to Fe (III)²⁴. The intensity ratio between the Fe (III) and Fe (II) peaks at 1.0 V *vs.* RHE for core-shell NPs is 0.59, slightly lower than the Fe (III)/Fe (II) intensity ratio of 0.61 observed for the Fe_3O_4 core NPs (Figure S9), pointing to smaller Fe (III) fraction on the surface of core-shell NPs compared to Fe_3O_4 NPs. The redox peaks of Figure 1B can be assigned with the help of the NEXAFS spectra. In the Fe L_3 -edge spectra measured at -0.2 *vs.* RHE (Figure 2 C), a significant increase of the Fe (II) peak and a pronounced decrease of the Fe (III) peak are clearly observed. Moreover, another shoulder at 706 eV, characteristic of the formation of FeO ²⁵, emerges at low potentials. These changes are accentuated at -0.5 V *vs.* RHE. Similar changes are also seen on the L_2 peaks at 720 eV, 722 eV, and 724 eV. Thus, a significant amount of the Fe (III) cations in the $CoFe_2O_4$ shell and also in the Fe_3O_4 core is reduced to FeO at potentials negative of the cathodic peak P_C . The Co L_3 -edge spectrum at 1V *vs.* RHE (Figure S10) displays 3 contributions between 777 and 784 eV and confirms the presence of Co (II) in the shell as

expected for CoFe_2O_4 . It should be mentioned that the Co $L_{2,3}$ -edge spectra are not modified even for potentials as low as -0.5 V vs. RHE , suggesting that Co (II) is not reduced at these potentials (Figure S11 A) while the O K-edge spectra evidenced some changes related to the transformation of the spinel structure into the wüstite structure (Figure S11 B). Furthermore, no signature corresponding to the reduction to metallic iron was observed in the NEXAFS spectra contrary to what has been reported in some previous publications²⁶).¹ When the potential is returned to its initial value (1.0 V vs. RHE), the Fe (II)/Fe (III) ratio returns to its initial value. Consequently, the chemical transformation of Fe (III) into Fe (II) and back appears reversible. Lastly, scanning TEM high angle annular dark-field (STEM-HAADF) micrographs and electron energy loss spectroscopy (EELS) STEM mappings before (Figure 1 D, 1E and 1F) and after (Figure 1 G, 1H and 1I) the application of -0.5 V vs. RHE for 30 min were studied. The results provide evidence for Co redistribution inside the core-shell NPs: before the application of a potential, the NPs present a high-density contrast between the core and the shell while after reduction they present a more homogeneous distribution of Co in the entire volume of the NPs. These differences likely result from the atomic diffusion inside the core and indicate that while being chemically reversible, the redox cycling results in some structural irreversibility of the core-shell NPs. Additional TEM micrographs of the NPs before and after reduction can be found in Figures S2 and S3. The important changes observed in the Fe $L_{2,3}$ -edge spectra underline that the NPs probed by the soft X-ray beam are electrically connected to the graphene bilayer, confirming that this spectro-

¹ Note that if the potential was scanned further negative, the CV became irreversible (not shown), which we tentatively attribute to the reduction of Fe_3O_4 to metallic Fe.

electrochemical cell design can be successfully utilized to assess changes occurring during the OER using *operando* NEXAFS.

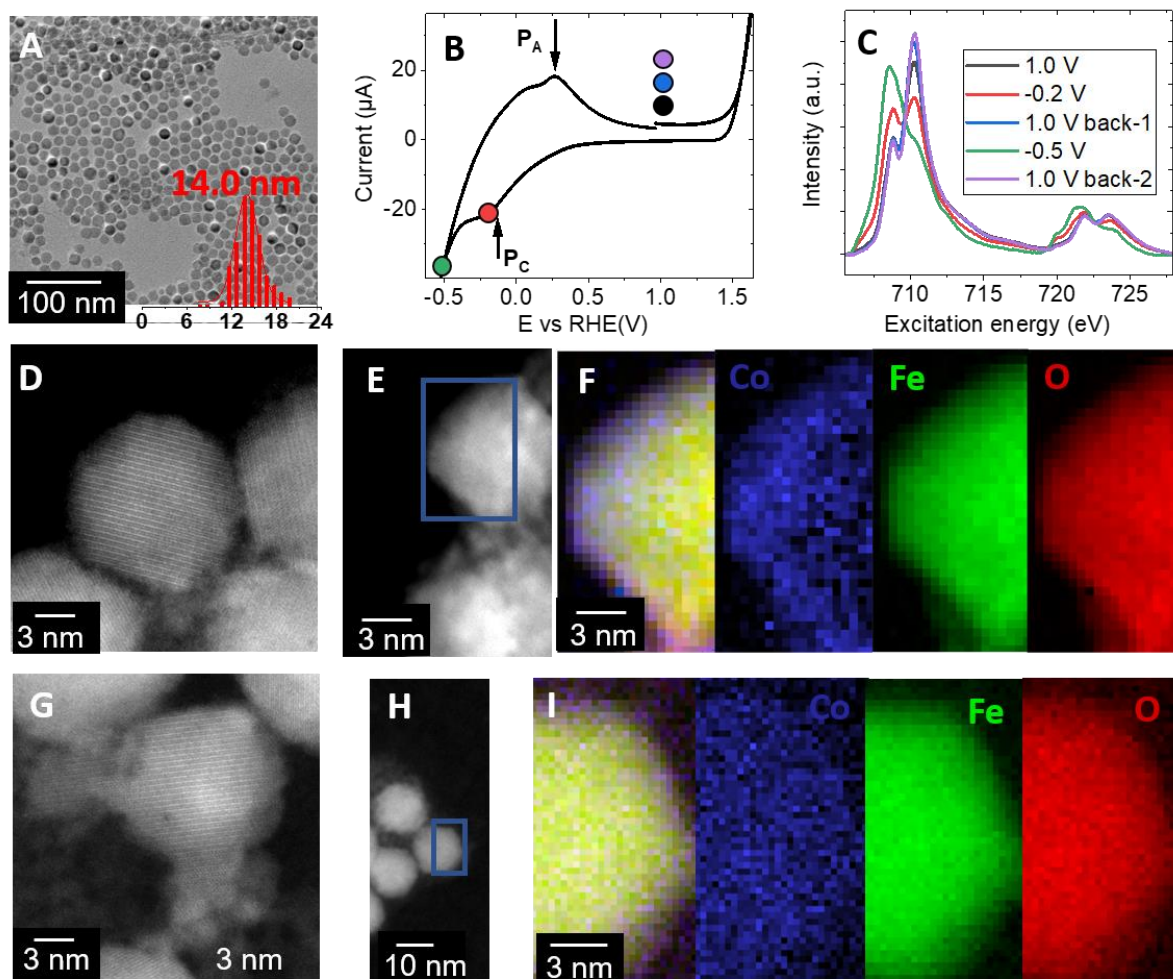


Figure 1: A) TEM image of the $\text{Fe}_3\text{O}_4@\text{CoFe}_2\text{O}_4$ core-shell NPs and their size distribution, average diameter 14 nm. B) Cyclic voltammetry curves of core-shell NPs acquired in a spectroelectrochemical cell with 0.1 M NaOH electrolyte at 20 mV s^{-1} scan rate. C) Area-normalized NEXAFS Fe- $L_{2,3}$ edge spectra for core-shell NPs at different applied potentials. All potentials are with respect to the RHE scale and are not *iR*-corrected. STEM-HAADF images of the NPs before (D and E) electrochemical measurements and after the application of -0.5 V vs. RHE for 30 min (G and H). F and I) Spatially-resolved EELS STEM analyses

of the core-shell NP from G) (before electrochemical measurements) and from H) (after application of -0.5 V vs. RHE for 30 min), correspondingly. Cobalt is colored blue; iron - green; and oxygen - red.

With this knowledge, we turn to the analyses of NEXAFS spectra acquired above 1.0 V vs. RHE. The cyclic voltammogram shown in Figure 2A shows a pair of low intensity peaks ($P_{A,1}$ and $P_{C,1}$) around 1.05 V vs. RHE, which are usually attributed to the Co (II/III) transition in Co_3O_4 or $Co(OH)_2$ materials^{5,6}. Additionally, a cathodic peak usually attributed to the Co (III/IV) transition^{5,6} is observed at higher positive potentials, around 1.3 V vs. RHE ($P_{C,2}$). The oxidation peak is hidden by the OER and is consequently barely distinguishable. Since the intensity of these CV peaks is low (compared to the peaks observed at low potentials), the changes in the NEXAFS spectra are expected to correspond to a minor oxidation change of the cations (Figure 2 B, C and D). The cyclic voltammetry curve obtained for Fe_3O_4 NPs does not exhibit these peaks around 1.1 and 1.4V.

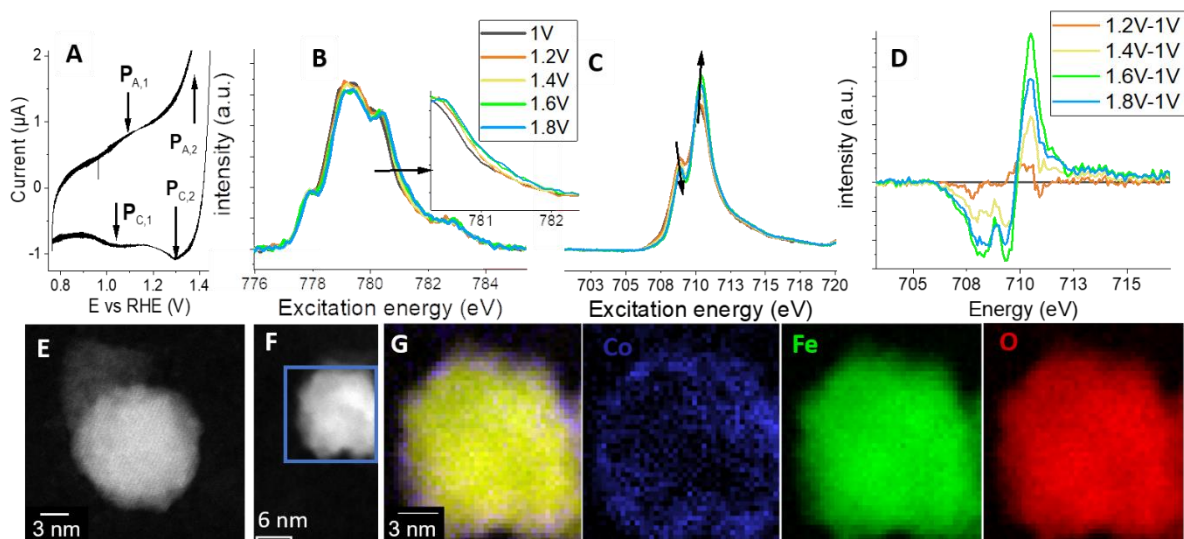


Figure 2: A) Cyclic voltammogram of $Fe_3O_4@CoFe_2O_4$ core-shell NPs acquired in a spectroelectrochemical cell in 0.1 M NaOH electrolyte at $20 \text{ mV} \cdot \text{s}^{-1}$ scan rate. Area-normalized Co-L₃ edge (B) and Fe-L₃ edge (C) NEXAFS spectra for core-shell NPs at different applied potentials. D) Fe-L₃ edge NEXAFS spectra to

which the spectrum at 1.0 V vs. RHE has been subtracted. STEM-HAADF images (E and F) and spatially-resolved EELS analyses (G) of core-shell NPs after the application of 1.75 V for 30 minutes. Cobalt is colored blue; iron - green; and oxygen - red. All potentials are with respect to the RHE scale and are not iR-corrected.

At 1.0 V vs. RHE, the Co L₃-edge NEXAFS spectrum exhibits a shape characteristic of Co (II). By comparing this spectrum with the simulated L_{2,3}-edges spectra of Co in Oh and Td sites²⁷, it is estimated that roughly 75% of cobalt resides in the Oh and 25% in the Td sites as expected for a mainly inverse spinel structure (Figure S10A). Surprisingly, when the potential is increased, in 0.2 V increments, up to 1.8 V vs. RHE (Figure 2B), the Co (II) signal is still largely present in NEXAFS spectra revealing that the spinel structure is preserved even under the OER conditions. However, it is worth noticing that the L₃ peak slightly shifts to higher energies when the applied potential increases, suggesting that a small fraction of Co (II) is transformed into Co (III) (see figure S10B for comparison with the published Co (II) and Co (III) L-edge spectra). Potential-induced changes observed at the Fe-L₃ edge (Figure 2C) are more significant with (i) the characteristic Fe (II)/Fe(III) peak ratio decreasing to 0.46 at 1.8 V vs. RHE and (ii) the disappearance of the 707 eV shoulder, both evidencing oxidation of a fraction of Fe (II) present in the NPs core into Fe(III)²⁸. As iron in the Fe (II) oxidation state is only present in the Fe₃O₄ core (in the shell it is Fe (III)), we conclude that the Fe₃O₄ core is strongly influencing the chemical properties of the CoFe₂O₄ shell, as this oxidation likely results from an electron transfer from the Fe (II) in the core to compensate for the Co oxidation and reduce the Co (III) species in the shell, essentially maintaining its Co (II) state. Additionally, STEM-HAADF micrographs and EELS mappings of the NPs after the oxidation (Figure 2 E, F and G) demonstrate that the crystallinity and the presence of the Co-containing shell have been preserved even after the application of 1.75

V *vs.* RHE for 30 minutes. Supplementary high-resolution TEM (HRTEM) micrographs of the NPs after oxidation can be found in Figure S4. However, the NPs appear to be rougher and the edges are not as sharp as before applying the anodic potential (Figure 2E). Such roughening may be tentatively attributed to the NP restructuring driven by the migration of excess Fe (III) cations from the core to the shell of the NPs. This hypothesis is supported by the reported evidence of the inverse spinel structure Fe₃O₄ (magnetite) that can easily transform into γ -Fe₂O₃ (maghemite) which is a deficient spinel, with vacancies in the octahedral sublattice²⁹. For example, oxidation of Fe (II) of magnetite NPs into Fe (III) by molecular oxygen involves electron hopping along with migration of Fe (III) cations through the lattice framework, generating vacancies in the octahedral sublattice (and their migration) in order to preserve the charge balance²⁹.

It is interesting to note that no changes were observed in the low excitation energy region of the O K-edge spectra when the potential was increased from 1.0 to 1.8 V *vs.* RHE (Figure S12). Thus, an anion redox mechanism involving the formation of an electrophilic oxygen species O⁻ as an OER intermediate can be discarded. On the other hand, a small peak around 714 eV emerges in the Fe L-edge spectra at $E > 1.6$ V *vs.* RHE (Figure 2 C and D) and may be tentatively attributed to the formation of Fe (IV), since broadening of the L₃ peak has been shown in the literature to correspond to Fe (IV)^{30,31}. Subtracting the spectrum obtained at 1 V *vs.* RHE from the spectra at higher potentials (Figure 2D) better highlights this peak. The presence of this peak agrees with a cation redox OER mechanism involving possible participation of Fe (IV) in the OER active site as it was suggested by Enman *et al.* upon *operando* hard-X-ray investigation of Co(Fe)O_xH_y oxyhydroxide³². Note that on the core alone (Fe₃O₄, Figure S9), which is much less OER-active and which has been proven to be stable during oxidation³³, almost no changes are seen on the Fe L-edge under the OER conditions. This hindered Fe₃O₄ core compared to Fe₃O₄@CoFe₂O₄ core-

shell NP oxidation may be attributed to the presence of a thin layer of $\gamma\text{-Fe}_2\text{O}_3$ on the surface of the Fe_3O_4 NPs acting as a passivating layer³⁰ and highlights the synergy between the Fe from the core and Co from the shell during the OER.

Considering this observation, we can conclude that in the core-shell NPs a small fraction of Fe (II) from the core, likely localized in the close proximity to the shell, is oxidized to Fe (III) to maintain the Co (II) state above 1.1 V vs. RHE. To preserve electroneutrality in the core, this Fe (III) cation probably migrates from the core towards the surface of the NPs, leaving behind a vacancy in the core and leading to a roughening of the NP surface. It is interesting to note that stabilization of the Co(II) state at high applied potential by the nearby Fe was already invoked in Refs. ^{15,16} dealing with DFT+U calculations of $\text{Co}_3\text{O}_4(001)$ and $\text{CoFe}_2\text{O}_4(001)$ surfaces with and without an additional half or full monolayer of Fe. It was concluded that the OER active site is octahedral Co, both in the presence and in the absence of a Fe monolayer. However, while for the Fe-free surface Co is oxidized to reach a Co(IV) state¹⁵, the presence of a Fe monolayer (for example, on the $\text{CoFe}_2\text{O}_4(001)$ surface) stabilizes the Co(II) state¹⁶, while itself relaxing to octahedral sites and accepting the Fe(III) oxidation state under the OER potential. In this case, the OER catalytic cycle would involve the oxidation of a surface active site composed of Co(II) interacting with a nearby Fe(III), into Co(III). The formation of short-lived Co (IV) as it has been suggested in the literature on similar compounds^{12,34} cannot be fully discarded. However, considering that only a small fraction of Co (II) is transformed into Co (III) during the OER, such a scenario is quite unlikely for the core-shell NPs. Finally, these results suggest that the anion redox mechanism previously proposed for IrO_x ^{8,9} and Co_3O_4 ¹⁸ anodes involving electron-deficient oxygen as an active intermediate is rather unlikely.

In addition, it is worth noticing that the spinel structure is preserved in the core as both Fe (II) and Fe (III) are present in the NPs at all potentials (*cf.* Figure 2C) as well as in the CoFe_2O_4 shell, where the Co is mainly resting in the Co(II) state (*cf.* Figure 2B), even at high potentials where the formation of cobalt oxyhydroxide phase has been previously found for Co_3O_4 .³⁻⁵

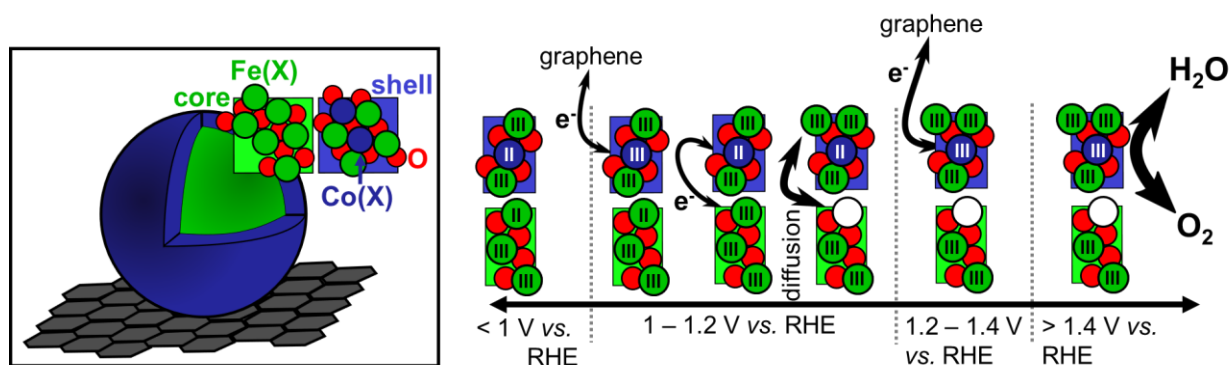


Figure 3: Proposed redox transformations on core-shell NPs depending on the applied potential. Step 1: At $E=1.0 \text{ V vs. RHE}$, Fe (II) and Fe (III) are coexisting in the core, and the shell is composed of Co (II) and Fe (III). Step 2: At $1.0 > E > 1.2 \text{ V vs RHE}$, an electron is transferred from Co (II) in the particle shell to the current collector. However, Co (III) is not observed by NEXAFS since it is reduced back to Co (II) due to an electron transfer from Fe (II) (residing in the NP core in the close proximity to the shell) resulting in the Fe (III) formation. This Fe (III) cation then likely migrates to the surface, leaving behind a cationic vacancy in the particle core. Step 3: Above 1.2 V vs RHE , Co (II) in the shell is partly oxidized to Co (III). Step 4: OER occurs on an active center comprised of Co (III) and Fe (III). However, one cannot exclude formation of active Fe (IV) species above 1.4 V vs RHE . Oxygen atoms are in red, cobalt in blue and iron in green.

To conclude, we performed an *operando* study using soft X-ray absorption spectroscopy over a wide potential range spanning from -0.5 V vs. RHE up to the OER interval on membrane

electrode assemblies containing cobalt iron oxide spinel core-shell nanoparticles ($\text{Fe}_3\text{O}_4@\text{CoFe}_2\text{O}_4$) covered by a graphene bilayer. This approach turns out to be well-suited for studying redox transformations of these NPs. The work sheds light onto the interactions between the core and the shell, providing insights into the synergies that might exist between the Fe in the core and the Co in the shell. We document a strong influence of the Fe_3O_4 core on the redox behavior of the CoFe_2O_4 shell under OER conditions. Compared to previously investigated Co_3O_4 or $\text{Co}(\text{OH})_2$ NPs³⁻⁶, core-shell $\text{Fe}_3\text{O}_4@\text{CoFe}_2\text{O}_4$ NPs behave differently: most of the cobalt atoms in the shell remain in a Co (II) oxidation state in the potential region where significant OER occurs. In addition, the presence of Co in the shell favors the oxidation of some fraction of Fe (II) into Fe (III) in the NPs core (in close proximity to the shell). Hence, these results suggest the occurrence of a cation-redox OER mechanism involving cooperative redox behavior between Co and Fe atoms. It is remarkable that the core-shell spinel structure is essentially preserved under the OER conditions but cannot withstand cathodic polarization to -0.5 V vs. RHE.

AUTHOR INFORMATION

Lisa Royer : lisa.royer@unistra.fr ICPEES, UMR 7515 CNRS-ECPM-Université de Strasbourg, 25, rue Becquerel, F 67087 Strasbourg Cedex 2, France,

Antoine Bonnefont : bonnefont@unistra.fr Institut de Chimie, UMR 7177, CNRS-Université de Strasbourg, 4 rue Blaise Pascal, CS 90032, 67081 Strasbourg cedex, France

Tristan Asset : t.asset@unistra.fr ICPEES, UMR 7515 CNRS-ECPM-Université de Strasbourg, 25, rue Becquerel, F 67087 Strasbourg Cedex 2, France

Benjamin Rotonelli: b.rottonelli@unistra.fr ICPEES, UMR 7515 CNRS-ECPM-Université de Strasbourg, 25, rue Becquerel, F 67087 Strasbourg Cedex 2, France

Juan Velasco Velez: velasco@fhi-berlin.mpg.de Fritz-Haber-Institute of the Max-Planck-Society, Faradayweg 4-6, 14195 Berlin, Germany/Department of Heterogeneous Reactions, Max Planck Institute for Chemical Energy Conversion, 45470 Mülheim an der Ruhr, Germany/ALBA Synchrotron Light Source, Cerdanyola del Vallés (Barcelona) 08290, Spain.

Benoit Pichon : benoit.pichon@unistra.fr IPCMS Université de Strasbourg, CNRS, Institut de Physique et Chimie des Matériaux de Strasbourg, UMR 7504, Strasbourg, F-67034 France /Institut Universitaire de France, 75231 Paris Cedex 05, France

Steven Holdcroft: holdcrof@sfu.ca Department of Chemistry, Simon Fraser University, 8888 University Drive, Burnaby, BC, V5A 1S6, Canada

Elena Savinova: elena.savinova@unistra.fr ICPEES, UMR 7515 CNRS-ECPM-Université de Strasbourg, 25, rue Becquerel, F 67087 Strasbourg Cedex 2, France

Simon Hettler: hettler@unizar.es Instituto de Nanociencia y Materiales de Aragon (INMA), CSIC-Universidad de Zaragoza, Calle Pedro Cerbuna 12, 50009 Zaragoza, Spain/ Laboratorio de Microscopías Avanzadas (LMA), Universidad de Zaragoza, Calle Mariano Esquillor, 50018 Zaragoza, Spain

Raul Arenal: arenal@unizar.es Instituto de Nanociencia y Materiales de Aragon (INMA), CSIC-Universidad de Zaragoza, Calle Pedro Cerbuna 12, 50009 Zaragoza, Spain/ Laboratorio de Microscopías Avanzadas (LMA), Universidad de Zaragoza, Calle Mariano Esquillor, 50018 Zaragoza, Spain/ARAID Foundation, 50018 Zaragoza, Spain

Notes

The authors declare no competing financial interests.

ASSOCIATED CONTENT

Supporting Information.

This information is available free of charge on the ACS Publications website

Experimental procedures, protocols for the synthesis of nanoparticles, preparation of membrane electrode assemblies, cyclic voltammetry of NPs, acquisition of diffractograms, NEXAFS measurements under applied potentials, Co L- edge under reduction potentials, O K-edge under reduction and oxidation potentials, HRTEM microscopy of NPs before and after the application of a potential (oxidation or reduction).

ACKNOWLEDGMENT

Project financially supported by the Foundation for frontier Research in chemistry. We thank the Helmholtz-Zentrum Berlin für Materialien und Energie for the allocation of synchrotron radiation beamtime and Fabrice Bournel and Jean Jacques Gallet for their help in the project. The authors would also like to thank the XRD platform of ICPEES and the TEM platform of IPCMS as well as V. Ramnarain for the HRTEM micrographs and B. Freis for the TEM micrographs. R.A. and S.H. acknowledge support from Spanish MICINN (PID2019-104739GB-I00/AEI/10.13039/501100011033), Government of Aragon (projects DGA E13-20R) and from EU H2020 “ESTEEM3” (Grant number 823717) and Graphene Flagship (881603). The STEM and EELS studies were performed in the Laboratorio de Microscopias Avanzadas (LMA), Universidad de Zaragoza (Spain).

REFERENCES

- (1) Thomas, O. D.; Soo, K. J. W. Y.; Peckham, T. J.; Kulkarni, M. P.; Holdcroft, S. Anion Conducting Poly(Dialkyl Benzimidazolium) Salts. *Polym. Chem.* **2011**, *2* (8), 1641–1643. <https://doi.org/10.1039/C1PY00142F>.
- (2) Holdcroft, S.; Fan, J. Sterically-Encumbered Ionenenes as Hydroxide Ion-Conducting Polymer Membranes. *Curr. Opin. Electrochem.* **2019**, *18*, 99–105. <https://doi.org/10.1016/j.coelec.2019.10.014>.
- (3) Bergmann, A.; Martinez-Moreno, E.; Teschner, D.; Chernev, P.; Gliech, M.; de Araújo, J. F.; Reier, T.; Dau, H.; Strasser, P. Reversible Amorphization and the Catalytically Active State of Crystalline Co₃O₄ during Oxygen Evolution. *Nat. Commun.* **2015**, *6* (1), 8625. <https://doi.org/10.1038/ncomms9625>.
- (4) Ortiz Peña, N.; Ihiawakrim, D.; Han, M.; Lassalle-Kaiser, B.; Carencó, S.; Sanchez, C.; Laberty-Robert, C.; Portehault, D.; Ersen, O. Morphological and Structural Evolution of Co₃O₄ Nanoparticles Revealed by in Situ Electrochemical Transmission Electron Microscopy during Electrocatalytic Water Oxidation. *ACS Nano* **2019**, *13* (10), 11372–11381. <https://doi.org/10.1021/acsnano.9b04745>.
- (5) Reikowski, F.; Maroun, F.; Pacheco, I.; Wiegmann, T.; Allongue, P.; Stettner, J.; Magnussen, O. M. Operando Surface X-Ray Diffraction Studies of Structurally Defined Co₃O₄ and CoOOH Thin Films during Oxygen Evolution. *ACS Catal.* **2019**, *9* (5), 3811–3821. <https://doi.org/10.1021/acscatal.8b04823>.
- (6) Mefford, J. T.; Akbashev, A. R.; Kang, M.; Bentley, C. L.; Gent, W. E.; Deng, H. D.; Alsem, D. H.; Yu, Y.-S.; Salmon, N. J.; Shapiro, D. A.; Unwin, P. R.; Chueh, W. C. Correlative Operando Microscopy of Oxygen Evolution Electrocatalysts. *Nature* **2021**, *593* (7857), 67–73. <https://doi.org/10.1038/s41586-021-03454-x>.
- (7) Haase, F. T.; Bergmann, A.; Jones, T. E.; Timoshenko, J.; Herzog, A.; Jeon, H. S.; Rettenmaier, C.; Cuenya, B. R. Size Effects and Active State Formation of Cobalt Oxide Nanoparticles during the Oxygen Evolution Reaction. *Nat. Energy* **2022**, 1–9. <https://doi.org/10.1038/s41560-022-01083-w>.
- (8) Pfeifer, V.; E. Jones, T.; Wrabetz, S.; Massué, C.; Vélez, J. J. V.; Arrigo, R.; Scherzer, M.; Piccinin, S.; Hävecker, M.; Knop-Gericke, A.; Schlögl, R. Reactive Oxygen Species in Iridium-Based OER Catalysts. *Chem. Sci.* **2016**, *7* (11), 6791–6795. <https://doi.org/10.1039/C6SC01860B>.
- (9) Saveleva, V. A.; Wang, L.; Teschner, D.; Jones, T.; Gago, A. S.; Friedrich, K. A.; Zafeirotos, S.; Schlögl, R.; Savinova, E. R. Operando Evidence for a Universal Oxygen Evolution Mechanism on Thermal and Electrochemical Iridium Oxides. *J. Phys. Chem. Lett.* **2018**, *9* (11), 3154–3160. <https://doi.org/10.1021/acs.jpcclett.8b00810>.
- (10) Feng, C.; Faheem, M. B.; Fu, J.; Xiao, Y.; Li, C.; Li, Y. Fe-Based Electrocatalysts for Oxygen Evolution Reaction: Progress and Perspectives. *ACS Catal.* **2020**, *10* (7), 4019–4047. <https://doi.org/10.1021/acscatal.9b05445>.

- (11) Li, M.; Gu, Y.; Chang, Y.; Gu, X.; Tian, J.; Wu, X.; Feng, L. Iron Doped Cobalt Fluoride Derived from CoFe Layered Double Hydroxide for Efficient Oxygen Evolution Reaction. *Chem. Eng. J.* **2021**, *425*, 130686. <https://doi.org/10.1016/j.cej.2021.130686>.
- (12) Wang, L.; Saveleva, V. A.; Eslamibidgoli, M. J.; Antipin, D.; Bouillet, C.; Biswas, I.; Gago, A. S.; Hosseiny, S. S.; Gazdzicki, P.; Eikerling, M. H.; Savinova, E. R.; Friedrich, K. A. Deciphering the Exceptional Performance of NiFe Hydroxide for the Oxygen Evolution Reaction in an Anion Exchange Membrane Electrolyzer. **2022**, *10*.
- (13) Xiao, H.; Shin, H.; Goddard, W. A. Synergy between Fe and Ni in the Optimal Performance of (Ni,Fe)OOH Catalysts for the Oxygen Evolution Reaction. *Proc. Natl. Acad. Sci.* **2018**, *115* (23), 5872–5877. <https://doi.org/10.1073/pnas.1722034115>.
- (14) Suntivich, J.; May, K. J.; Gasteiger, H. A.; Goodenough, J. B.; Shao-Horn, Y. A Perovskite Oxide Optimized for Oxygen Evolution Catalysis from Molecular Orbital Principles. *Science* **2011**, *334* (6061), 1383–1385. <https://doi.org/10.1126/science.1212858>.
- (15) Peng, Y.; Hajiyani, H.; Pentcheva, R. Influence of Fe and Ni Doping on the OER Performance at the Co₃O₄(001) Surface: Insights from DFT+U Calculations. *ACS Catal.* **2021**, *11* (9), 5601–5613. <https://doi.org/10.1021/acscatal.1c00214>.
- (16) Hajiyani, H.; Pentcheva, R. Surface Termination and Composition Control of Activity of the Co_xNi_{1-x}Fe₂O₄(001) Surface for Water Oxidation: Insights from DFT+U Calculations. *ACS Catal.* **2018**, *8* (12), 11773–11782. <https://doi.org/10.1021/acscatal.8b00574>.
- (17) Calvillo, L.; Carraro, F.; Vozniuk, O.; Celorrio, V.; Nodari, L.; Russell, A. E.; Debellis, D.; Fermin, D.; Cavani, F.; Agnoli, S.; Granozzi, G. Insights into the Durability of Co–Fe Spinel Oxygen Evolution Electrocatalysts via Operando Studies of the Catalyst Structure. *J. Mater. Chem. A* **2018**, *6* (16), 7034–7041. <https://doi.org/10.1039/C7TA10892C>.
- (18) Saddeler, S.; Bendt, G.; Salamon, S.; Haase, F. T.; Landers, J.; Timoshenko, J.; Rettenmaier, C.; Jeon, H. S.; Bergmann, A.; Wende, H.; Cuenya, B. R.; Schulz, S. Influence of the Cobalt Content in Cobalt Iron Oxides on the Electrocatalytic OER Activity. *J. Mater. Chem. A* **2021**, *9* (45), 25381–25390. <https://doi.org/10.1039/D1TA06568H>.
- (19) Strickler, A. L.; Escudero-Escribano, M.; Jaramillo, T. F. Core–Shell Au@Metal-Oxide Nanoparticle Electrocatalysts for Enhanced Oxygen Evolution. *Nano Lett.* **2017**, *17* (10), 6040–6046. <https://doi.org/10.1021/acs.nanolett.7b02357>.
- (20) Zhuang, Z.; Sheng, W.; Yan, Y. Synthesis of Monodisperse Au@Co₃O₄ Core-Shell Nanocrystals and Their Enhanced Catalytic Activity for Oxygen Evolution Reaction. *Adv. Mater.* **2014**, *26* (23), 3950–3955. <https://doi.org/10.1002/adma.201400336>.
- (21) Sartori, K.; Musat, A.; Choueikani, F.; Grenèche, J.-M.; Hettler, S.; Bencok, P.; Begin-Colin, S.; Steadman, P.; Arenal, R.; Pichon, B. P. A Detailed Investigation of the Onion Structure of Exchanged Coupled Magnetic Fe₃-δO₄@CoFe₂O₄@Fe₃-δO₄ Nanoparticles. *ACS Appl. Mater. Interfaces* **2021**, *13* (14), 16784–16800. <https://doi.org/10.1021/acami.0c18310>.

- (22) Falling, L. J.; Mom, R. V.; Sandoval Diaz, L. E.; Nakhaie, S.; Stotz, E.; Ivanov, D.; Hävecker, M.; Lunkenbein, T.; Knop-Gericke, A.; Schlögl, R.; Velasco-Vélez, J.-J. Graphene-Capped Liquid Thin Films for Electrochemical Operando X-Ray Spectroscopy and Scanning Electron Microscopy. *ACS Appl. Mater. Interfaces* **2020**, *12* (33), 37680–37692. <https://doi.org/10.1021/acsami.0c08379>.
- (23) Streibel, V.; Hävecker, M.; Yi, Y.; Velasco Vélez, J. J.; Skorupska, K.; Stotz, E.; Knop-Gericke, A.; Schlögl, R.; Arrigo, R. In Situ Electrochemical Cells to Study the Oxygen Evolution Reaction by Near Ambient Pressure X-Ray Photoelectron Spectroscopy. *Top. Catal.* **2018**, *61* (20), 2064–2084. <https://doi.org/10.1007/s11244-018-1061-8>.
- (24) Sassi, M.; Pearce, C. I.; Bagus, P. S.; Arenholz, E.; Rosso, K. M. First-Principles Fe L_{2,3}-Edge and O K-Edge XANES and XMCD Spectra for Iron Oxides. *J. Phys. Chem. A* **2017**, *121* (40), 7613–7618. <https://doi.org/10.1021/acs.jpca.7b08392>.
- (25) Regan, T. J.; Ohldag, H.; Stamm, C.; Nolting, F.; Lüning, J.; Stöhr, J.; White, R. L. Chemical Effects at Metal/Oxide Interfaces Studied by x-Ray-Absorption Spectroscopy. *Phys. Rev. B* **2001**, *64* (21), 214422. <https://doi.org/10.1103/PhysRevB.64.214422>.
- (26) Accogli, A.; Bertoli, L.; Panzeri, G.; Gibertini, E.; Pesce, R.; Bussetti, G.; Magagnin, L. Electrochemical Characterization of Magnetite (Fe₃O₄) Nanoaggregates in Acidic and Alkaline Solutions. *ACS Omega* **2021**, *6* (41), 26880–26887. <https://doi.org/10.1021/acsomega.1c03142>.
- (27) Papaefthimiou, V.; Dintzer, T.; Dupuis, V.; Tamion, A.; Tournus, F.; Hillion, A.; Teschner, D.; Hävecker, M.; Knop-Gericke, A.; Schlögl, R.; Zafeirotos, S. Nontrivial Redox Behavior of Nanosized Cobalt: New Insights from Ambient Pressure X-Ray Photoelectron and Absorption Spectroscopies. *ACS Nano* **2011**, *5* (3), 2182–2190. <https://doi.org/10.1021/nn103392x>.
- (28) Zhou, S.; Potzger, K.; Xu, Q.; Kuepper, K.; Talut, G.; Markó, D.; Mücklich, A.; Helm, M.; Fassbender, J.; Arenholz, E.; Schmidt, H. Spinel Ferrite Nanocrystals Embedded inside ZnO: Magnetic, Electronic, and Magnetotransport Properties. *Phys. Rev. B* **2009**, *80* (9), 094409. <https://doi.org/10.1103/PhysRevB.80.094409>.
- (29) Jolivet, J.-P.; Tronc, E.; Chanéac, C. Iron Oxides: From Molecular Clusters to Solid. A Nice Example of Chemical Versatility. *Comptes Rendus Geosci.* **2006**, *338* (6), 488–497. <https://doi.org/10.1016/j.crte.2006.04.014>.
- (30) Ikeno, H.; Tanaka, I.; Miyamae, T.; Mishima, T.; Adachi, H.; Ogasawara, K. First Principles Calculation of Fe L_{2,3}-Edge X-Ray Absorption Near Edge Structures of Iron Oxides. *Mater. Trans.* **2004**, *45* (5), 1414–1418. <https://doi.org/10.2320/matertrans.45.1414>.
- (31) Abbate, M.; de Groot, F. M. F.; Fuggle, J. C.; Fujimori, A.; Strebel, O.; Lopez, F.; Domke, M.; Kaindl, G.; Sawatzky, G. A.; Takano, M.; Takeda, Y.; Eisaki, H.; Uchida, S. Controlled-Valence Properties of La_{1-x}Sr_xFeO₃ and La_{1-x}Sr_xMnO₃ Studied by Soft-x-Ray Absorption Spectroscopy. *Phys. Rev. B* **1992**, *46* (8), 4511–4519. <https://doi.org/10.1103/PhysRevB.46.4511>.

- (32) Enman, L. J.; Stevens, M. B.; Dahan, M. H.; Nellist, M. R.; Toroker, M. C.; Boettcher, S. W. Operando X-Ray Absorption Spectroscopy Shows Iron Oxidation Is Concurrent with Oxygen Evolution in Cobalt–Iron (Oxy)Hydroxide Electrocatalysts. *Angew. Chem. Int. Ed.* **2018**, *57* (39), 12840–12844. <https://doi.org/10.1002/anie.201808818>.
- (33) Müllner, M.; Riva, M.; Kraushofer, F.; Schmid, M.; Parkinson, G. S.; Mertens, S. F. L.; Diebold, U. Stability and Catalytic Performance of Reconstructed Fe₃O₄(001) and Fe₃O₄(110) Surfaces during Oxygen Evolution Reaction. *J. Phys. Chem. C* **2019**, *123* (13), 8304–8311. <https://doi.org/10.1021/acs.jpcc.8b08733>.
- (34) Smith, R. D. L.; Pasquini, C.; Loos, S.; Chernev, P.; Klingan, K.; Kubella, P.; Mohammadi, M. R.; Gonzalez-Flores, D.; Dau, H. Spectroscopic Identification of Active Sites for the Oxygen Evolution Reaction on Iron-Cobalt Oxides. *Nat. Commun.* **2017**, *8* (1), 2022. <https://doi.org/10.1038/s41467-017-01949-8>.